Mn-POROUS SILICATES AS PROMISING CATALYSTS FOR METHANE COMBUSTION

Amal BEJAR [a], Semy BEN CHAABENE [a], Latifa BERGAOUI [a,b]

[a] *Laboratory of Materials Chemistry and Catalysis, Faculty of Sciences of Tunis, El Manar University, Tunis, Tunisia.*
[b] *Department of Biological and Chemical Engineering, National Institute of Applied Sciences and Technology, Carthage University, Tunis, Tunisia.*

(Submitted: 20 September 2015, accepted: 26 October 2015)

ABSTRACT: The present study aims to evaluate the catalytic performance of synthetic minerals containing manganese, for methane combustion. Al-Mn-silicate nanobubbles and Mn-zeolite (analcime) were first hydrothermally synthesized using the *one-pot* method. The thermal stability of an Al-Mn-silicate nanobubbles sample was studied. Elaborated solids were characterized by powder X-ray diffraction, N_2-physisorption, Fourier transformed infrared spectroscopy, ^{27}Al and ^{29}Si magic angle spinning nuclear magnetic resonance and transmission electron microscopy and tested in methane combustion. Catalytic tests have shown that the conversion strongly depends on the nature of used mineral. Catalytic performances are controlled by both acidic and redox properties of the catalyst. Interesting activity, selectivity and stability were recorded for Al-Mn-silicate nanobubbles. These results may encourage the development of Mn-porous minerals as promising catalysts for methane combustion. They may be the best alternative to replace noble metals based catalysts which are characterized by their poor resistance to deactivation and their high cost.

Keywords: Mn-analcime, Al-Mn-silicate nanobubbles, hydrothermal synthesis, methane combustion.

RESUME: Le présent travail porte sur l'évaluation des performances catalytiques des minéraux de synthèse riches en manganèse dans la réaction de combustion du méthane. Des nanobulles d'aluminosilicate de manganèse et une Mn-zéolithe (analcime) ont été préparés par voie hydrothermale. La stabilité thermique de l'échantillon nanobulles d'aluminosilicate de manganèse a été étudiée. Les solides élaborés ont été caractérisés par diverses techniques physico -chimiques, à savoir la diffraction des rayons X, la physisorption d'azote, la spectroscopie infrarouge à transformée de Fourier, la résonance magnétique nucléaire en rotation à l'angle magique des noyaux ^{27}Al et ^{29}Si et la microscopie électronique à transmission. Ils ont été par la suite testés dans la combustion du méthane. Les différents tests catalytiques ont montré que la conversion dépend de la nature du minéral utilisé. Les performances catalytiques ont été reliées aux propriétés acides et redox des catalyseurs. Les nanobulles d'aluminosilicate de manganèse ont montré une activité, une sélectivité et une stabilité intéressantes. Ces résultats encouragent le développement de minéraux poreux riches en manganèse en tant que catalyseurs prometteurs pour la combustion du méthane. Ils constituent une bonne alternative pour remplacer les catalyseurs à base de métaux nobles qui sont caractérisés par leur faible résistance à la désactivation et par leur coût élevé.

Mots clés : Mn-analcime, nanobulles d'aluminosilicate de manganèse, synthèse hydrothermale, combustion du méthane.

INTRODUCTION

Methane (CH_4) is considered as one of the most dangerous air pollutants [1]. It is roughly twenty five times more potent as a greenhouse gas than carbon dioxide (CO_2) [2]. As it causes the warming of atmosphere, methane has a human health, economic and environmental impact. This gas has both natural and human sources. More than 60 % of CH_4 emissions [3] are related to different human activities (industry sector, land feels treatment, burning of fossils and agriculture activities…). Emissions containing hydrocarbons have to be in all cases channeled and treated and there are

* Corresponding author, e-mail address : latifa.bergaoui@insat.rnu.tn

a number of ways to reduce these emissions. In industry, two main processes are used to remove organic compounds: catalytic and non-catalytic oxidation. For CH_4, the catalytic method is believed to be the best alternative since the oxidation of CH_4 is quite difficult [2,4]. The methane combustion has an important added value which is energy production [5]. For these reasons, the catalytic combustion process has attracted researchers' attention. Two groups of catalysts were developed for this purpose: noble and transition metals based catalysts. Noble metals supported materials present high activities [6] but a poor resistance to poisoning, a quick deactivation and a high cost [1,7,8]. Transition metal based materials are less active but more resistant to thermal and coke deactivation [2,9]. They are also abundant and cheaper than noble metals based materials [10]. Among various transition metals, manganese is considered as one of the best candidates for catalytic methane combustion [11,12]. As it has several stable oxidation degrees, manganese shows outstanding redox properties [5]. The catalytic activity of manganese is usually correlated to the reducible Mn^{n+1}/Mn^{n+} content [11,13]. Moreover, high oxidation states are very suitable to obtain great conversions. Indeed, it was reported that Mn^{4+} species are more active than Mn^{3+} [5]. The use of suitable support for these catalytic sites can enhance catalytic performance. In this aim, porous materials (zeolites, clays and silica) were frequently used due to their attractive properties [4,14,15]. They provide a high surface area, a high metal dispersion, an acidic surface and sometimes a great thermal stability. However, these minerals exhibit some drawbacks. The stabilization of active centers using several methods (grafting, ion exchange and impregnation) remains quite inefficient. For example the deposition of Mn on SiO_2 surface gives a very weak interaction between the active sites and the silica [16]. In the case of clay minerals, high temperature induces layers collapse which makes the active sites inaccessible. For zeolites, a high Si/Al ratio is required to ensure the thermal stability of catalysts [17] while a low Si/Al ratio promotes the binding of cations. Preparing adequate catalysts remains an important challenge in order to satisfy expected properties, improve catalytic selectivity and enhance support stability. To achieve these goals herein we report the "*one-pot*" preparation of Mn-porous materials. In fact, recently we are interested in the synthesis of aluminum silicate rich in manganese. In this work, Al-Mn-silicate nanobubbles (AMS) and an analcime-type Mn-zeolite were synthesized by hydrothermal method and characterized. Catalytic performances of obtained minerals were then investigated and compared in the methane combustion reaction.

EXPERIMENTAL PART

1. Hydrothermal synthesis of minerals

Different minerals (Al-Mn-silicate nanobubbles and Mn-analcime) were prepared by mixing silicic acid (Sigma Aldrich, purity: 99.9%), manganese (II) carbonate (Sigma Aldrich, purity: 99.9%) and aluminum nitrate nonahydrate (Acros, purity: 99.9%) with an aqueous solution of NaOH (Acros, purity: pure pellets). The final volume of the prepared suspensions was 15 mL and the capacity of the used Teflon-lined stainless steel Parr reactors was 25 mL. Mn-analcime was prepared following the hydrothermal protocol proposed by Bejar *et al.*[18]. 160 mg of silicic acid, 280 mg of $Al(NO_3)_3.9H_2O$, 160 mg of $MnCO_3$ and 240 mg of NaOH were mixed with distilled water. The hydrothermal treatment was performed at 175°C for 48 h. The solid was separated from aqueous solution by centrifugation, washed several times with distilled water and finally dried overnight at 60°C. The hydrothermal synthesis of Al-Mn-silicate nanobubbles was performed at 140°C during 48 h using 50.62 mg of silicic acid, 60 mg of NaOH and different amounts of Al $(NO_3)_3.9H_2O$ and $MnCO_3$. The Mn/(Al+Mn) molar ratio was varied from 0 to 1 (0, 0.35, 0.65, 0.85 and 1). All chemicals were mixed with distilled water. Obtained mineral,

designed as MSN, was recovered by centrifugation, washed several times with distilled water and dried overnight at 60°C. MSN catalysts were calcined at different temperatures in oxygen. Calcined samples were named MSN_T, where T is the treatment temperature.

2. Minerals characterization

Siemens D-500 X-ray diffractometer, with CuKα radiation was used to identify the crystalline phases.The diffractograms were recorded in the 5-70° 2θ range with a step size of 2° min^{-1}. Nitrogen physisorption analyses were performed on a Micromeritics ASAP 2020M. Specific surface areas were estimated by the BET method. Transmission electron microscopy (TEM- JEOL100CX) was used to observe the morphologies of MSN and Mn-analcime. FT-IR spectra were collected on KBr pellets in the region 4000-400 cm^{-1} using a Nicolet IR200 spectrometer (Thermo Scientific). ^{29}Si and ^{27}Al Magic Angle Spinning Nuclear Magnetic Resonance (MAS-NMR) spectra were carried out on a Bruker 300WB spectrometer (B_0=7.1 T) operating at 78.2 MHz with a spinning frequency of 8 kHz using TMS and $AlCl_3.6H_2O$ as references, respectively. The single-pulse duration and the recycle delay were 5 µs and 5 s, respectively. The average oxidation state of manganese was determined by titration. The test consists in dissolving 10 mg of the mineral in a solution containing NaI (4 mol L^{-1}) and NaOH (8 $mol.L^{-1}$), heating the solution to 40°C and adding 2 mL of concentrated H_2SO_4. The manganese oxidizes the iodide ions to iodine, which is titrated by sodium thiosulfate (0.25 mol. L^{-1}).

3. Catalytic application

The catalytic combustion of methane corresponds to its conversion into carbon dioxide and water. For this purpose, a quartz fixed-bed reactor containing 100 mg of the catalysts was used. The solids were firstly pretreated in oxygen at 600°C for 1 h. The methane combustion tests were then performed using continuous-flow method in the presence of gas mixtures of He grade-A, CH_4 (10% in Ar) and O_2 grade-A, with flow rates 100, 10 and 4 $cm^3.min^{-1}$, respectively. The reaction was conducted at atmospheric pressure. The temperature was decreased from 600°C by steps until obtaining a zero activity. The products were analyzed every 30 minutes by an Intersmat IGC gas chromatograph equipped with a thermal conductivity detector and a Porapak Q column. The temperature of the oven, injector and detector were 100, 120 and 120°C, respectively.

Since all tested catalysts were very selective to CO_2 and H_2O, the conversion was calculated as follow:

$$\text{Conversion (\%)} = 100\ \frac{P(CO_2)}{P(CH_4)+P(CO_2)}$$

$P(CO_2)$ and $P(CH_4)$ are measured partial pressures of CO_2 and CH_4 respectively.

RESULTS AND DISCUSSION

1. Characterization of prepared minerals

Al-Mn-silicate nanobubbles (MSN)

TEM photographs of Al-Mn-silicate nanobubbles are given in Figure 1. Micrographs show the presence of many aggregates of "bubbles" (hollow spheres). The sphere diameter varies from 8 to 10 nm while the shell thickness is around 0.7 nm. Similar nanobubble structures systems have been recently reported [19,20]. Some traces of lamellar phases were also detected. The

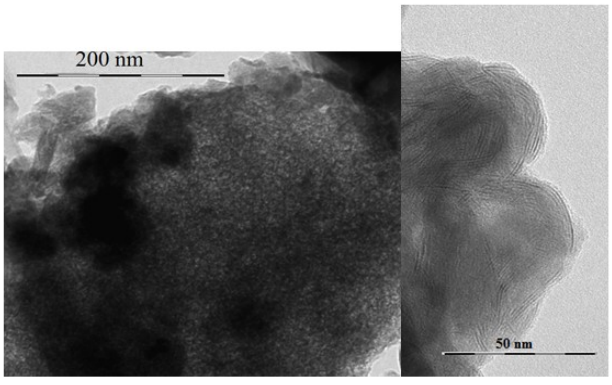

a **b**

Figure 1. TEM images showing two different morphologies: (a) bubble like-morphology (most abundant) and (b) lamellar structure.

thickness of the observed layers is about 0.7 nm. Nanobubbles have an amorphous structure [19]. They only present a very broad reflection at 2θ angles between 30 and 35° when analyzed by XRD. The examination of XRD pattern of MSN (Figure 2-a) shows a significant background noise indicating that a large fraction of the sample is amorphous. Reflections at 7.1 Å and 3.2 Å are assigned to the minority lamellar phases observed by TEM. They could correspond either to a TO clay type kaolinite [21] and/or to birnessite type MnO_2 [22]. Moreover, diffractograms reveal unreacted $MnCO_3$ (minor phase) at 2.82 Å and 1.76 Å.

The infrared spectrum of MSN is shown in Figure 2-b. The broad band at around 3435 cm^{-1} and the band at about 1628 cm^{-1} are assigned to water molecules. The band at 1406 cm^{-1} is attributed to the C-O stretching vibration of unreacted carbonate ions [23]. Bands at 1010 cm^{-1} and 453 cm^{-1} correspond to the Si-O-Si stretching vibrations (ν_s and ν_{as}) [24]. Bands at 749 cm^{-1} and 600 cm^{-1} are probably due to the ν_s T-O-T (T= Si or Al) [25,26].

Solid-state ^{27}Al and ^{29}Si MAS NMR spectra of MSN are reported in Figure 3. Broad peaks are observed. The origin of this broadening is probably caused by the presence of paramagnetic centers Mn^{x+} in the vicinity of ^{27}Al and ^{29}Si nuclei. The ^{27}Al MAS NMR spectrum (Figure 3-a) shows a single broad peak at about 55 ppm attributed to aluminum in tetrahedral coordination [27]. The ^{29}Si MAS NMR spectrum (Figure 3-b) presents a broad resonance with a maximum at -93 ppm. It is typical of Si in Q^3 environments with different numbers of Al neighbors.

The average oxidation state of manganese in the MSN structure was determined by the iodometric titration. Experimental results showed an average value of 3.6. Thus, Mn^{4+} is

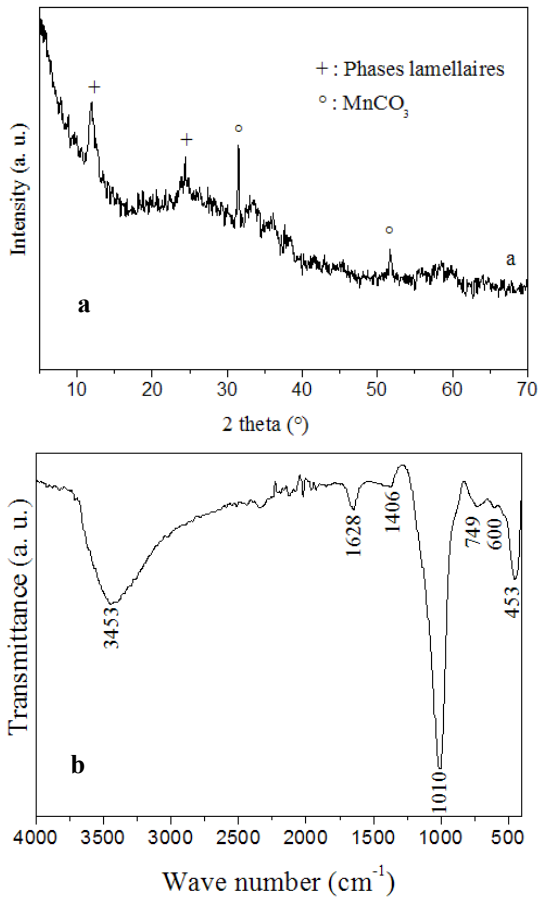

Figure 2. XRD pattern (a) and FTIR spectrum (b) of prepared MSN

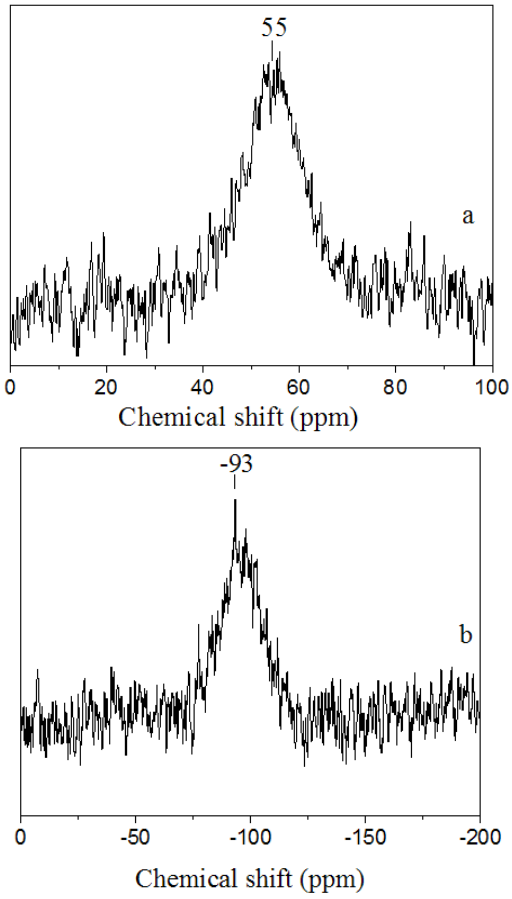

Figure 3. MAS NMR spectra of MSN of (a) ^{27}Al and (b)^{29} Si.

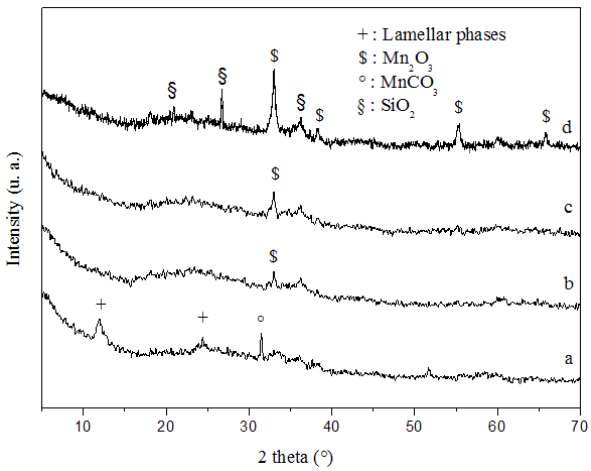

Figure 4. XRD patterns of: (a) MSN, (b) MSN_{600}, (c) MSN_{650} and (d) MSN_{700}.

the majority species with an amount of lower oxidation states. Different combinations of Mn^{4+} with Mn^{2+} and/or Mn^{3+} could account for the experimental result. In those Mn-Al-Si systems, walls seem to be made by Mn^{3+}, Mn^{4+}, Al^{3+} and Si^{4+} cations in tetrahedral positions. Mn^{3+}/Si^{4+} and Al^{3+}/Si^{4+} substitutions in the tetrahedral lattice usually generate a significant negative layer charge and consequently an important cationic exchange capacity. In our previous work, we have reported that Al-Mn-silicate nanobubbles present a cationic exchange capacity around 243 meq/100g which is saturated by Mn^{2+} [20].

The effect of calcination temperature on the structure and the texture of MSN was also investigated. The XRD patterns of MSN_T given in Figure 4; show that the thermal treatment causes the disappearance of characteristic reflections of the lamellar structures at 7.1 and 3.4 Å. The literature reports that kaolinite becomes amorphous from 550°C [28] while lamellar birnessite turns into another structure from 600°C [29]. New reflections assigned to Mn_2O_3 manganese oxide are observed. Their relative intensities become sharper for the highest calcination temperatures. For MSN_{700} sample, the formation of silica (quartz) can be even noted. The N_2 adsorption/desorption isotherms of MSN_T samples are shown in Figure 5.

Table I. The effect of calcination temperature on BET surface area.

Samples	Surface area (m^2/g)
None calcined	175
MSN_{600}	60
MSN_{650}	65
MSN_{700}	57

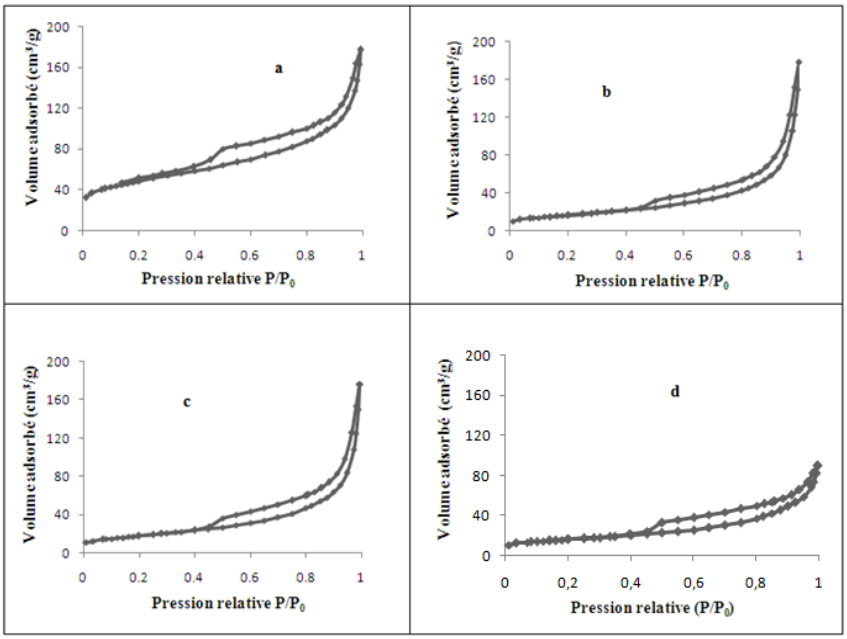

Figure 5. 77 K Nitrogen adsorption-desorption isotherms at 77 K of: (a) MSN, (b) MSN_{600}, (c) MSN_{650} and (d) MSN_{700}.

Thermal treatment does not alter the global form of adsorption/desorption isotherms. All of them are of type IV with a hysteresis loop of type H3, which is typical of slit-shaped and/ or inkbottle pores [30].
The BET surface areas of MSN samples before and after calcination at different temperatures are given in Table I. The BET specific surface area drops from 175 to around 60 m^2/g. The agglomeration of bubbles and the formation of more compact structures are probably the main causes of this surface area decrease.

2. Mn-analcime

Figure 6-a shows that a well-crystallized analcime was obtained by hydrothermal synthesis. The weak peak at 7.1 Å ($2\theta \approx 12°$) is assigned to minority lamellar phases. It was reported that lamellar structures (kaolinite, birnessite and/or halloysite) are intermediates to the formation of analcime [18].
TEM image of Mn-analcime sample (Figure 7) presents many aggregates with intra particular porosity. The average oxidation state of manganese estimated by iodometric titration is about 3.8. In our previous work, we have proven by several methods that Mn-analcime contains 80% of Mn^{4+} and 20% of Mn^{3+} [20]. Both Mn^{4+} and Mn^{3+} substitute tetrahedral silicon in the zeolite framework. There was no evidence of extra-framework manganese traces. Na^+ seems to act as compensating

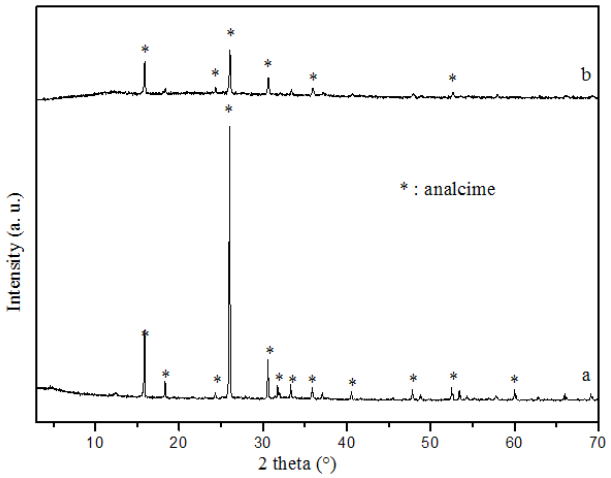

Figure 6. XRD patterns of Mn-analcime before (a) and after (b) calcination.

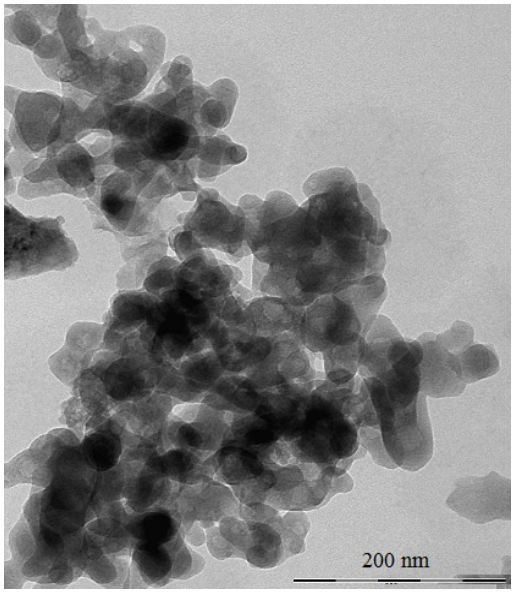

Figure 7. TEM image of Mn-analcime.

cations with a cationic exchange capacity estimated to 277 meq/100g.
The thermal stability of Mn-analcime was investigated. The synthetic zeolite was calcined at 650°C in order to be used as a catalyst for the methane combustion. XRD pattern (Figure 6-b) shows that this mineral is thermally stable. The corresponding reflections are maintained even after calcination at 650°C which indicates that the three-dimensional architecture is retained. Nevertheless, the BET surface area decreases from 180 m^2/g to 25 m^2/g after calcination. This decrease is probably caused by the agglomeration of particles and the closing of the porosity.

3. Catalytic combustion of CH_4

3.1. Catalytic activities of MSN and MSN_T

The catalytic performances of MSN and MSN_T were investigated. Figure 8 represents the evolution of CH_4 conversion performed at 600°C (reaction temperature) during 150 min using MSN_T catalysts. Histograms show that the activity of the different minerals increases gradually with time and then stabilizes after 30 min indicating that a steady state is reached. The catalytic activity remains stable with time (over more than 150 min). All catalysts are stable and the manganese seems to be resistant

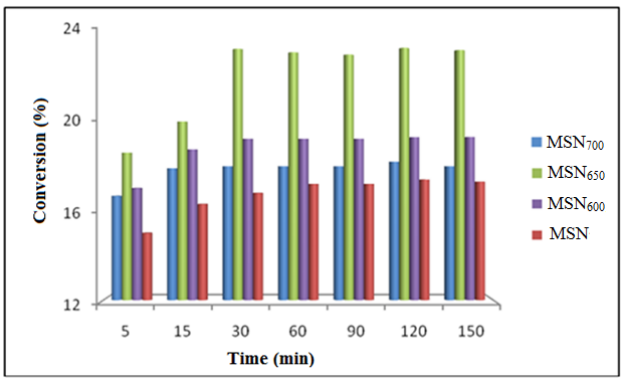

Figure 8. Methane conversion at 600°C using MSN calcined at different temperatures.

to the deactivation and poisoning. In addition, the obtained conversions show that the catalytic performance is strongly depending on the calcination conditions. The activity gradually increases from MSN to MSN_{650} and then decreases for MSN_{700}. In fact, such an evolution cannot be related to surface area evolution (specific surface area dropped with calcination temperature). It seems that a thermal treatment promotes substantial transformations on the nanobubbles structure giving rise to suitable active sites for methane combustion. However, the decrease noted in the case of MSN_{700} could be attributed to the formation of both silica and manganese oxides which suggest the complete decomposition of nanobubbles and consequently the active centers loss.

The CH_4 conversion results calculated for the MSN_T catalysts at different reaction temperatures during the steady state are shown in Figure 9. As it can be observed, the highest activities are measured for a calcination temperature of 650°C. Moreover, MSN_{650} exhibits a measurable activity from 420°C whereas other catalysts are inactive below 440°C. For this reason, a calcination temperature of 650°C was chosen in all the following tests. MSN_{600}, MSN_{650} and MSN_{700} curves (Figure 9-b, c and d) show a first plateau region at low conversion values, for temperature below 500°C. These behaviors could mean that there are probably two different types of active sites.

3.2. The effect of Mn/(Mn+Al) ratio on the catalytic activity

The active sites content is one of the most important parameters which can affect the performance and the behavior of a catalyst. Making the hypothesis that active sites are correlated with the presence of Mn, the concentration of Mn was varied during hydrothermal synthesis of MSN-like samples. The used Mn/(Mn+Al) molar ratios are 0, 0.35, 0.65, 0.85 and 1. As it can be seen in Figures 10 and 11, the sample prepared with the molar ratio Mn/(Mn+Al) equal to 0.65 is the most active. The Mn-free catalyst (Mn/(Mn+Al) = 0) is inactive. It is believed that Mn centers are crucial for the progress of methane oxidation. In addition, the sample prepared with no aluminum (Mn/(Mn+Al) = 1) is slightly active. It was reported, in supported palladium system, that the presence of some *Lewis* acid centers is recommended for the methane combustion reaction [2]. However,

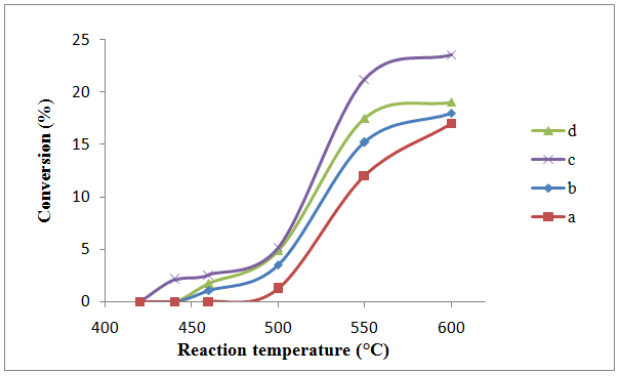

Figure 9. Influence of temperature on methane conversion during the steady state using MSN_T catalysts: (a) MSN, (b) MSN_{600}, (c) MSN_{650} and (d) MSN_{700}.

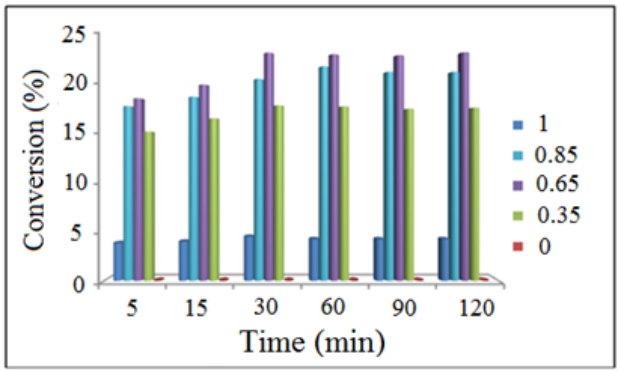

Figure 10. Methane conversion at 600°C using samples prepared with different Mn/(Mn+Al) molar ratios.

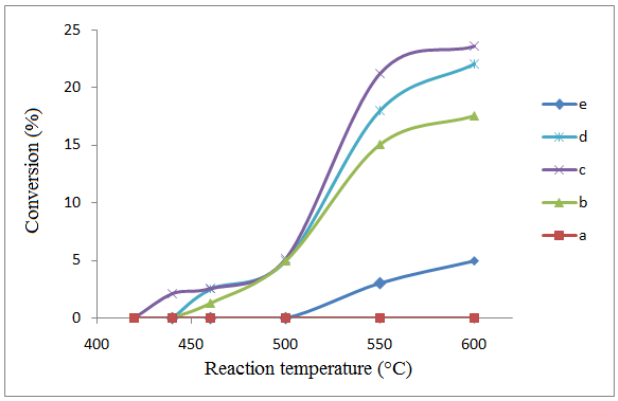

Figure 11. Influence of temperature on methane conversion during the steady state using catalysts prepared with various Mn/(Mn+Al) molar ratios (a) 0, (b) 0.35, (c) 0.65, (d) 0.85 and (e) 1.

strong support acidity could inhibit the oxidation process. The electron withdrawing properties of *Lewis* centers may suppress the activity of loaded metallic sites [4,15]. A compromise must thus be found. In our case, this problem does not arise due to the *one-pot* synthesis method which provides stable manganese species. In order to study the influence of aluminum content on the methane combustion, the sample prepared with a lack of aluminum nitrate (Mn/(Mn+Al) = 1) was slightly ground in the presence of a commercial aluminum oxide. The obtained solid was then calcined at 650°C and finely evaluated in the methane combustion at 600°C. As expected, conversion was improved. It increased from 4% to 28% in the presence of aluminum oxide.

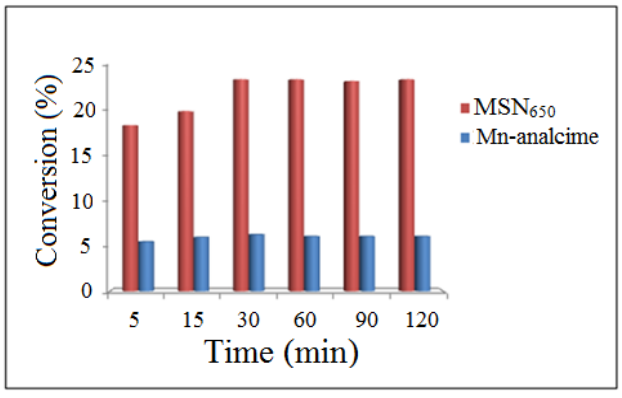

Figure 12. Methane conversion at 600°C using MSN_{650} and calcined Mn-analcime.

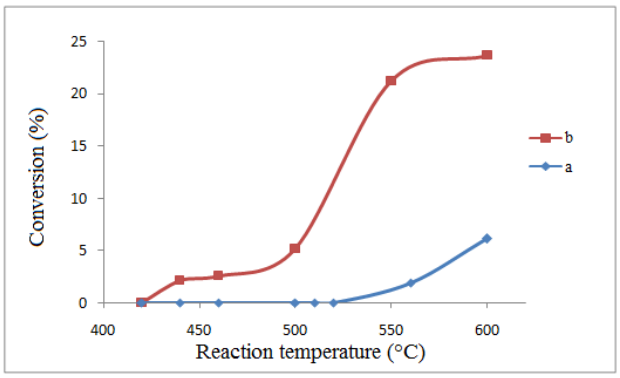

Figure 13. Influence of temperature on methane conversion during the steady state using: (a) calcined Mn-analcime and (b) MSN_{650}.

3.3. The influence of the mineral structure on the catalytic activity (Mn-analcime and MSN)

In order to study the influence of the mineral structure on the catalytic performances, Mn-analcime was used. For this purpose and to compare the activity of this zeolite to MSN, Mn-analcime was calcined at 650°C and then tested in the methane combustion. Measured conversions at 600°C are summarized on Figure 12.

The obtained data show that the zeolite exhibits a lower activity as compared to MSN_{650}. Indeed after 2 h, the conversion of MSN_{650} was higher than that of Mn-analcime by about 3.6 times. It can be confirmed that the nature of the support strongly affects the catalytic behavior of active sites. This result is also proved by the study of the evolution of the conversion in the steady state at different reaction temperatures (Figure 13).

Several causes could explain the difference between these behaviors: (1) the structural and chemical composition, (2) the aluminum concentration, (3) the manganese oxidation state, (4) the manganese coordination, (5) the presence of Mn^{2+} as extra-framework cations in the MSN structure and (5) the textural properties. Further studies are needed to discriminate between these hypotheses. We note here, that the obtained activities in the CH_4 combustion on Mn rich minerals remain lower than these obtained with supported palladium systems [6,31,32].

CONCLUSION

In this study, Mn-analcime and Al-Mn-silicate nanobubbles were prepared as promising catalysts for methane combustion. For this purpose, the original *one-pot* preparation method was used. The Adopted hydrothermal synthesis provides improved manganese dispersion and stable oxidation states. Interesting activity, stability and selectivity were recorded for Al-Mn-silicate nanobubbles while Mn-analcime was less active. The difference between these two minerals was explained by textural and structural properties. It was also observed that the catalytic performance is controlled by both acidic and redox properties. Adding a small amount of aluminum to the prepared Mn-silicate mineral could significantly enhance the activity. Hence, there is a synergetic effect between the redox centers and the acid sites. Despite their relatively low activities, Mn-porous minerals could replace commonly conventional catalysts due to their higher poisoning resistance, higher selectivity and lower cost.

REFERENCES

[1] M.M. Fiuk, a. Adamski, *Catal. Today*, **2015**, 257 Part 1, 131..

[2] E. Asedegbega-Nieto, E. Díaz , A. Vega, S. Ordóñez, *Catal. Today*, **2010**, 157, 425.

[3] B. Anderson, K. Barlett, S. Frolking, K. Hayhoe, J. Jenkins, W. Salas, *Methane and nitrous oxide emissions from natrual sources*, pp. 1–194, United States Environmental Protection Agency, Office of Atmospheric Programs, Washington, **2010**.

[4] H. Maeda, Y. Kinoshita, K.R. Reddy, K. Muto, S. Komai, N. Katada, M. Niwa, *Appl. Catal.* A, **1997**, 163, 59.

[5] J. Hu, W. Chu, L. Shi, *J. Natural Gas Chem.*, **2008**, 17, 159.

[6] M. Saïd Zina, A. Ghorbel, *Solid State Sci.*, **2004**, 6, 973.

[7] C. Liu, H. Xian, Z. Jiang, L. Wang, J. Zhang, L. Zheng, Y. Tan, X. Li, *Appl. Catal.* B, **2015**, 176, 542.

[8] Y. Ozawa, Y. Tochihara, A. Watanabe, M. Nagai, S. Omi, *Appl. Catal.* A, **2004**,259, 1.

[9] V. A. de la Peña O'Shea, M.C. Alvarez-Galvan, J. Requies, V.L. Barrio, P.L. Arias, J.F. Cambra, M.B. Güemez, J.L.G. Fierro, *Catal. Commun.*, **2007**, 8, 1287.

[10] J. Li, X. Liang, S. Xu, J. Hao, *Appl. Catal.* B, **2009**,90, 307.

[11] A. Machocki, T. Ioannides, B. Stasinska, W. Gac, G. Avgouropoulos, D. Delimaris, W. Grzegorczyk, S. Pasieczna, *J. Catal.*, **2004**, 227, 282.

[12] T. V. Choudhary, S. Banerjee, V.R. Choudhary, *Appl. Catal.* A, **2002**, 234, 1.

[13] P. Artizzu-Duart, Y. Brullé, F. Gaillard, E. Garbowski, N. Guilhaume, M. Primet, *Catal. Today,* **1999**, 54, 181.

[14] Z. Jiang, J. Yu, J. Cheng, T. Xiao, M.O. Jones, Z. Hao, P.P. Edwards, *Fuel Process. Technol.*, **2010**, 91, 97.

[15] K. Okumura, S. Matsumoto, N. Nishiaki, M. Niwa, *Appl. Catal.* B, **2003**, 40, 151.

[16] H. Einaga, S. Yamamoto, N. Maeda, Y. Teraoka, *Catal. Today*, **2014**, 242, 287.

[17] G. Cruciani, J. Phys. Chem. Solids, **2006**, 67, 1973.

[18] A. Bejar, S. Ben Chaabene, M. Jaber, J.F. Lambert, L. Bergaoui, *Micropor. Mesopor. Mat.*, **2014**, 196, 158.

[19] C.C. Yec, H.C. Zeng, ACS Nano, **2014**, 8, 6407.

[20] A. Bejar, S. Ben Chaabene, M. Jaber, J.F. Lambert, L. Bergaoui. Accepted for publication in Applied Clay Science.

[21] J. Choi, S. Komarneni, M. Park, *Appl. Clay Sci.*, **2009**, 44, 237.

[22] M. Tsuda, H. Arai, Y. Sakurai, J. *Power Sources*, **2002**, 110, 52.

[23] S. Stojkovikj, M. Najdoski, V. Koleva, S. Demiri, *J. Phys. Chem. Solids*, **2013**, 74, 1433.

[24] Á.A.B. Maia, R.S. Angélica, R. de Freitas Neves, H. Pllmann, C. Straub, K. Saalwächter, *Appl. Clay Sci.*, **2014**, 87, 189.

[25] R. Dimitrijevic, V. Dondur, *J. Solid State Chem.*, **1995**, 115, 214.

[26] B.S. Liu, D.C. Tang, C.T. Au, *Micropor. Mesopor. Mat.*, **2005**, 86, 106.

[27] A.B. Pinar, R. Verel, J. Pérez-Pariente, J.A. Van Bokhoven, *Micropor. Mesopor. Mat.*, **2014**, 193, 111.

[28] J.B. Dixon, M.L. Jackson, *Science*, **1959**, 129, 1616.

[29] O. Prieto, M. Del Arco, V. Rives, *Thermochim. Acta*, **2003**, 401, 95.

[30] T. Novaković, L. Rožić, S. Petrović, A. Rosić, *Chem. Eng. J.*, **2008**, 137, 436.

[31] M. Hoffmann, S. Kreft, G. Georgi, G. Fulda, M. M. Pohl, D. Seeburg, C. Berger-Karin, E. V. Kondratenko, S. Wohlrab, Appl. Catal. B, **2015**, 197, 313.

[32] F. F. Muñoz, R. T. Baker, A. G. Leyva, R. O. Fuentes, *Appl. Catal.* B, **2013**, 136, 122.